

# A novel Zn-indiffused mode converter in x-cut lithium niobate

Ruey-Ching Twu<sup>1\*</sup>, Hsuan-Hsien Lee<sup>2</sup>, Hao-Yang Hong<sup>1</sup>, and Chin-Yau Yang<sup>1</sup>

<sup>1</sup>*Department of Electro-Optical Engineering, Southern Taiwan University  
1, Nan-Tai St., Yung-Kang City, Tainan 710, Taiwan, R.O.C.*

<sup>2</sup>*Department of Electrical Engineering, Southern Taiwan University  
1, Nan-Tai St., Yung-Kang City, Tainan 710, Taiwan, R.O.C.*

\*[rctwu@mail.stut.edu.tw](mailto:rctwu@mail.stut.edu.tw)

**Abstract:** A novel Zn-indiffused mode converter has been proposed and experimentally studied in an x-cut/z-propagation lithium niobate at a wavelength of 0.632  $\mu\text{m}$  for the first time. The optimized phase-matching and mode-conversion voltages for maximum conversion are 12 V and  $-5$  V, respectively. The results show that the proposed mode converter can operate with a stable conversion efficiency of about 99.5% between TM and TE polarizations at a throughput power of 25  $\mu\text{W}$  in a period of 60 min. Moreover, a comparison of optical power-handling stability between the Ti-indiffused and the Zn-indiffused channel waveguides, was explored. The encouraging results indicate that the Zn-indiffused waveguide has better power stability than the Ti-indiffused waveguide. Thus, it is expected that the proposed mode converter will have better stability than the conventional Ti-indiffused ones, especially in the visible wavelength region.

©2007 Optical Society of America

**OCIS codes:** (130.3120) Integrated optics devices; (230.2090) Electro-optical devices; (160.3730) Lithium niobate.

---

## References and links

1. C. Li, X. Cui, I. Yamaguchi, M. Yokota, and T. Yoshino, "Optical voltage sensor using a pulse-controlled electrooptic quarter waveplate," *IEEE Trans. Instrum. Meas.* **54**, 273-277 (2005).
2. R. C. Alferness, "Electrooptic guided-wave device for general polarization transformations," *IEEE J. Quantum Electron.* **17**, 965-969 (1981).
3. S. Thaniyavarn, "Wavelength independent, optical damage immune z-propagation LiNbO<sub>3</sub> waveguide polarization converter," *Appl. Phys. Lett.* **47**, 674-677 (1985).
4. T. Kawazoe, K. Satoh, I. Hayashi, and H. Mori, "Fabrication of integrated-optic polarization controller using z-propagating Ti-LiNbO<sub>3</sub> waveguides," *J. Lightwave Technol.* **10**, 51-56 (1992).
5. R. C. Alferness and L. L. Buhl, "Tunable electro-optic waveguide TE-TM converter/wavelength filter," *Appl. Phys. Lett.* **40**, 861-862 (1982).
6. N. A. Sanford, J. M. Connors, and W. A. Dyes, "Simplified z-propagating DC bias stable TE-TM mode converter fabricated in y-cut lithium niobate," *J. Lightwave Technol.* **6**, 898-901 (1988).
7. T. J. Wang, W. S. Lin, and F. K. Liu, "Integrated-optic biosensor by electro-optically modulated surface plasmon resonance," *Biosens. Bioelectron.* **22**, 1441-1446 (2007).
8. Y. Fujii, Y. Otsuka, and A. Ikeda, "Lithium niobate as an optical waveguide and its application to integrated optics," *IEICE Trans. Electron.* **E90-C**, 1081-1089 (2007).
9. T. Fujiwara, S. Sato, H. Mori, and Y. Fujii, "Suppression of crosstalk drift in Ti: LiNbO<sub>3</sub> waveguide switches," *J. Lightwave Technol.* **6**, 909-915 (1988).
10. H. Nagata, K. Kiuchi, S. Shimotsu, and J. Ogiwara, "Estimation of direct current bias and drift of Ti: LiNbO<sub>3</sub> optical modulators," *J. Appl. Phys.* **76**, 1405-1408 (1994).
11. Y. Kong, J. Wen, and H. Wang, "New doped lithium niobate crystal with high resistance to photorefractive-LiNbO<sub>3</sub>:In," *Appl. Phys. Lett.* **66**, 280-281 (1995).
12. T. Fujiwara, R. Srivastava, X. Cao, and R. V. Ramaswamy, "Comparison of photorefractive index change in proton-exchanged and Ti-diffused LiNbO<sub>3</sub> waveguides," *Opt. Lett.* **18**, 346-348 (1993).
13. J. D. Bull, Nicolas A. F. Jaeger, and F. Rahmatian, "A new hybrid current sensor for high-voltage applications," *IEEE Trans. Power Del.* **20**, 32-38 (2005).

14. B. M. Haas and T. E. Murphy, "A simple, linearized, phase-modulated analog optical transmission system," *IEEE Photon. Technol. Lett.* **19**, 729-731 (2007).
  15. R. C. Twu, "Zn-diffused 1×2 balanced-bridge optical switch in a y-cut lithium niobate," *IEEE Photon. Technol. Lett.* **19**, 1269-1271 (2007).
  16. I. Suárez, R. Matesanz, I. Aguirre de Cárcer, P. L. Pernas, F. Jaque, R. Blasco, and G. Lifante, "Antibody binding on LiNbO<sub>3</sub>:Zn waveguides for biosensor applications," *Sens. Actuators B-Chem.* **107**, 88-92 (2005).
  17. Ming, C. B. E. Gawith, K. Gallo, M. V. O'Connor, G. D. Emmerson, and P. G. R. Smith, "High conversion efficiency single-pass second harmonic generation in a zinc-diffused periodically poled lithium niobate waveguide," *Optics Express* **13**, 4862-4868 (2005).
- 

## 1. Introduction

The control of a polarization state of an incident light wave is essential for the applications of optical metrology and optical communication systems. In the buck-optics, the polarization states can be changed by using a polarization controller, which normally consists of a polarizer, a half-wave plate, and a quarter-wave plate. Usually, this setup needs an additional server control to change the relative angles between the polarizer and wave plates. However, the mechanical controls have limitations on the measurement's precision and speed. Because of the optical birefringent properties, an electrooptic (EO) crystal can be electrooptically controlled through EO coefficients. The electrically driving wave plates and phase modulators have been also demonstrated in the Pockels crystal of lithium niobate (LN) for the optical voltage sensor, in which a highly applied voltage ( $> 100$  V) is necessary [1]. To make a compact module with a lower driving voltage, a Ti-indiffused (TI) waveguide mode converter for mode conversion was successfully demonstrated in an LN substrate [2, 3]; various device forms based on these structures have appeared, including a polarization scrambler and a controller [2, 4]. In principle, the mode conversion between the orthogonal TE and TM components is achieved electrooptically by utilizing an off-diagonal element of the EO tensor to cause mixing between the orthogonal and normally uncoupled TE and TM modes [3]. There are two different kinds of mode converters in the LN waveguides. One is wavelength dependent with a narrow bandwidth, which was demonstrated in an x-cut/y-propagation or a z-cut/y-propagation waveguide with the finger electrodes [5, 2]. It can also be used as a wavelength filter. The other mode converter is wavelength independent with a broad-band conversion, which was fabricated in an x-cut/z-propagation or a y-cut/z-propagation waveguide, with parallel electrodes [3, 6]. The z-propagation mode converters, in which both polarizations see the same index ( $n_o$ : ordinary refractive index of LN substrate). The only birefringence is a small modal birefringence. Moreover, the optical damage due to photorefractive effects was known to be much less susceptible in comparison with those of y-propagations [3].

Traditionally, most of the commercial LN-related products operating in the infrared wavelengths (1.32–1.55  $\mu\text{m}$ ) were widely used in fiber optical communications. Recently, the capability of EO performance has also been employed for the waveguide-type bio-sensors [7]. Because the LN waveguides easily suffer from optical damage in the visible wavelengths, the input power levels are limited even in the infrared wavelengths under high irradiated powers [8]. The bias conditions of EO modulators are unstable due to the drift phenomenon of the photo-excited carriers, the permittivity differences between the substrate, and the buffer layer material [9, 10]. Moreover, the distortion of the transmitted light spot under higher laser intensities has been observed in [11]. Thus, the optical power stability in the channel waveguide is dependent on the photorefractive effects.

In the optical sensor applications, a He-Ne laser of 0.632- $\mu\text{m}$  wavelength is often used as a light source. To obtain operation stability during optical measurements, it is essential to use a stable waveguide device with enough throughput power to provide a sufficient signal-to-noise ratio to the received photo-detectors. Although a proton-exchanged (PE) waveguide has a higher resistance to optical damage than the TI waveguide [12], the PE waveguides support only an inherently extraordinary polarization, which cannot be applied to a dual-polarization guiding device such as a polarization phase modulator [13, 14] or a mode converter. Thus, it

has been recently pointed out that the Zn-indiffused (ZI) Mach-Zehnder modulators and bio-sensing waveguides were successfully fabricated by using a metallic and a vapor-phase Zn-indiffusion in LN substrates, respectively [15, 16]. In comparison with the conventional TI waveguides, the properties of dual-polarization guiding as well as less optical damage on the z-cut ZI waveguides have also been reported in [17].

In this paper, the metallic ZI mode converter is successfully demonstrated in the x-cut/z-propagation LN substrate at a wavelength of  $\lambda=0.632 \mu\text{m}$ , for the first time. Similar to the device structure as proposed in [3], a three-parallel-electrodes structure is employed, the center of which overlays a length of the waveguide channel. In this structure, phase matching is obtained when a bias voltage is applied between the outer electrodes through the EO coefficients of  $r_{12}$  and  $r_{22}$  ( $r_{12} = -r_{22}$ ) while a voltage, applied between the center and outer electrodes, forces a mode conversion through the EO coefficient  $r_{61}$ . The measured conversion efficiency, from the input TM polarization to the output TE polarization, is of about 99.5%. The stability of mode conversion was tested with a throughput power of  $25 \mu\text{W}$  in a period of 60 min under electrical driving, and it shows that the conversion is stable by using optimized applied voltages for phase matching and mode conversion. Besides, a comparison of optical power-handling stability between the TI and the ZI channel waveguides was also explored, and the results show that the ZI waveguide has better stability and a higher throughput power than the TI waveguide, especially in the visible wavelength region.

## 2. Device principles and fabrications

The device structure for top and cross section views are depicted in Fig. 1(a) and (b), respectively.

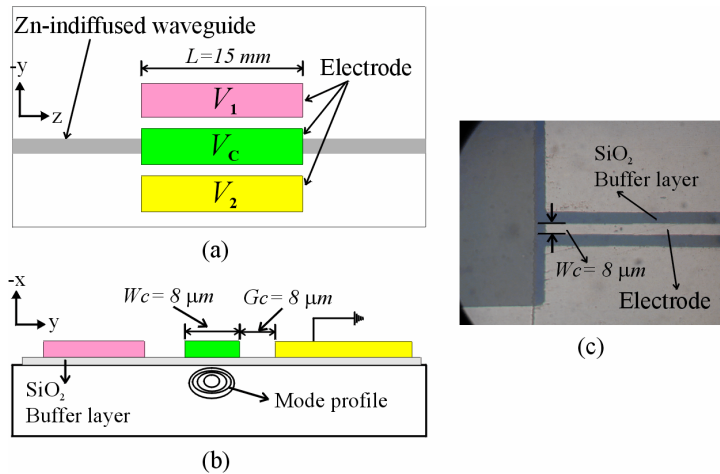


Fig. 1. Device structures for (a) top view, (b) cross section view, and (c) surface photography of fabricated devices.

The geometry of this device consists of a channel waveguide of  $4 \mu\text{m}$ -wide and  $22 \text{ mm}$ -long with three parallel electrodes, which was formed parallel to the  $z$  axis on the  $-x$  surface of LN substrate. The central electrode width  $W_C$  is  $8 \mu\text{m}$ ; the electrode gaps  $G_C$  between the center and the two outer electrodes are also  $8 \mu\text{m}$ . The length of electrodes  $L$  is  $15 \text{ mm}$ . One of the outer electrodes  $V_2$  is grounded ( $V_2 = 0 \text{ V}$ ), and two independent voltages  $V_C$  and  $V_1$  can be applied to the center and the other outer electrode, respectively. According to the similar formulas reported in [4], we assume that the incident light launched into the mode converter to be in the TM polarization, and the corresponding output powers of TM- and TE-polarized can be written as

$$P_{TM} = 1 - \frac{\kappa^2}{\kappa^2 + \delta^2} \sin^2 \left( \sqrt{\kappa^2 + \delta^2} L \right) \quad (1)$$

$$P_{TE} = \frac{\kappa^2}{\kappa^2 + \delta^2} \sin^2 \left( \sqrt{\kappa^2 + \delta^2} L \right) \quad (2)$$

where  $\kappa$  and  $\delta$  can be expressed as linear functions of applied voltages  $V_C$ ,  $V_1$ , and the initial modal birefringence  $\Delta\beta$  as shown in the following

$$\kappa = (\pi \Gamma_1 n_o^3 r_{61} / \lambda G_C) \cdot (V_C - V_1 / 2) \quad (3)$$

$$\delta = \Delta\beta / 2 + (\pi \Gamma_2 n_o^3 r_{22} / (2G_C + W_C)) \cdot V_1 \quad (4)$$

Where  $\Gamma_1$  and  $\Gamma_2$  are the overlap integrals of the electric and optical fields.

To fabricate a single-mode waveguide for both TE and TM polarizations, a 35 nm Zn film with a predeposition Ni film of 6 nm was deposited over the substrate *via* e-beam evaporation. Then, the waveguide pattern was formed by a lift-off technique. After the thermal diffusion of 850°C for 150 min, the substrate end faces were polished, and a silicon dioxide (SiO<sub>2</sub>) buffer layer of 300 nm was deposited. Then, an Al electrode thickness of 300 nm was deposited and patterned. The top-view photography of the fabricated device shows a good alignment process in the electrode region as shown in Fig. 1(c).

### 3. Characteristics of the Zn-indiffused mode converter

The He-Ne laser light source of 0.632  $\mu\text{m}$  was coupled into the front-end face of the waveguide with an input coupling lens (40 $\times$ ), and the output beam was imaged onto a Si photodetector or a charge-coupled device (CCD) camera with an output coupling lens (40 $\times$ ). The measured near-field profiles of both the TE and TM modes for the initial input and the converted modes under optimized applying voltages (will be explained later) are shown in Fig. 2.

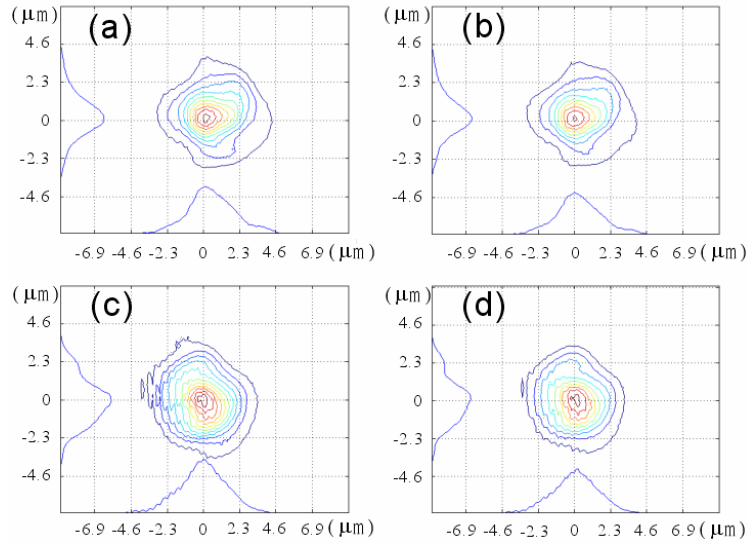


Fig. 2. Near-field profiles for (a) the initial input TE mode, (b) the converted TM-polarized mode with TE-polarized input, (c) the initial input TM mode, and (d) the converted TE-polarized mode with TM-polarized input.

The mode sizes (full width at half maximum power intensity) were  $2.9 \mu\text{m}$  (width)  $\times$   $2.4 \mu\text{m}$  (depth),  $2.8 \mu\text{m} \times 2.3 \mu\text{m}$  for the initial input TE mode (Fig. 2(a)) and the converted TM mode (Fig. 2(b)), respectively. The mode sizes were  $2.8 \mu\text{m} \times 2.9 \mu\text{m}$ ,  $2.8 \mu\text{m} \times 2.8 \mu\text{m}$  for the initial input TM mode (Fig. 2(c)) and the converted TE mode (Fig. 2(d)), respectively. The measured mode sizes can be further used for calculations of power density and overlap integral. The optimized switching voltages for maximum mode conversion efficiency were determined by measuring the corresponding relations between input electrical signals and output optical response curves.

Figure 3 shows the conversion characteristics of input TM-polarized mode versus a continuous saw-tooth voltage  $V_C$  with a frequency of 10 Hz under different voltages  $V_1$  at  $V_2 = 0$  V. According to Eq. (1) and Eq. (2), the maximum mode conversion is dependent on the values of  $\kappa$  and  $\delta$ . To achieve a complete conversion from input TM polarization to output TE polarization, the phase matching between TM and TE modes can be achieved by using the optimized voltages at  $V_1 = 12$  V ( $V_2 = 0$  V) as seen in Fig. 3(c). The conversion efficiency of about 99.5% is obtained at  $V_C = +6$  V,  $V_C = -5$  V, and the conversion characteristics are also similar to the results reported in [4]. Therefore, the voltage required for TM/TE conversion is about 5.5 V.

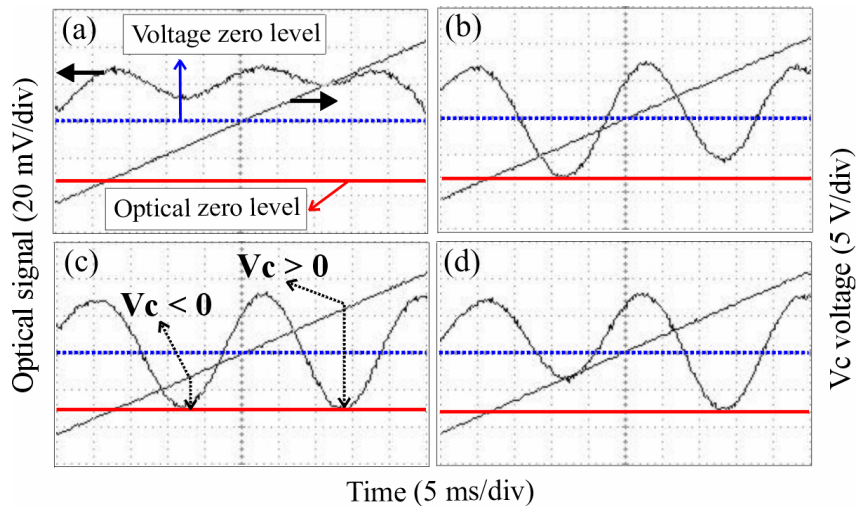


Fig. 3. Conversion characteristics of input TM-polarized mode versus  $V_C$  voltages under different phase-matching voltages  $V_1$ . (a)  $V_1 = 0$  V, (b)  $V_1 = 8$  V, (c)  $V_1 = 12$  V, and (d)  $V_1 = 16$  V.

#### 4. Photorefractive effects on the device performance

Figure 4 shows the long-term stability measurements under a throughput power of  $25 \mu\text{W}$  measuring after the output coupling lens at the wavelength of  $0.632 \mu\text{m}$ . At an applied constant voltage of  $V_1 = 12$  V, and a continuous saw-tooth voltage  $V_C$  with a frequency of 10 Hz, the maximum conversion is gradually reduced as an increase of illuminating time at the applied voltage of  $V_C = +6$  V. However, the maximum conversion is stable at the applied voltage of  $V_C = -5$  V. The mechanism of a time-dependent change on the conversion efficiency can be explained according to Fig. 5. Basically, the layered structures of  $V_C$  electrode, silicon dioxide, and LN substrate are similar to that of a metal-oxide-semiconductor (MOS) device. In the case of  $V_C > 0$  ( $V_C = +6$  V), there are negatively voltage-induced charges, which accumulated under the  $\text{SiO}_2$  layer, and near the top edge of the waveguide mode. At the same time, the negatively photo-excited carriers that generated from the  $\text{Fe}^{2+}$  sites, due to

photorefractive effects, will be spatially separated under a bias difference between  $V_1$  and  $V_2$ . The nonuniform distributions of the photo-excited carriers can produce a net electric field to reduce the electric field strength driven by the external applied voltage  $V_1$ . Therefore, the conversion efficiency is gradually reduced from 99.5% to 81.2% over an illuminating time of 60 min, because of the finally effective voltages are not the original phase-matching conditions ( $V_C = +6$  V and  $V_1 = 12$  V). This means that the amount of the photo-excited carriers is increased as well as the illuminating time. At the measured time of 50 min, the final efficiency of about 83.7% is close to the result shown in Fig. 3(b). Obviously, the photo-excited carriers make an equalized voltage reduction of about 4 V for the originally applied voltage  $V_1$ . However, in the case of  $V_C < 0$  ( $V_C = -5$  V), the positively voltage-induced charges can possibly trap most of the photo-excited carriers. There is no induced electric field to reduce the electric field driven by the applied voltages  $V_1$ . Thus, the unchanged phase-matching conditions can maintain a stable mode conversion.

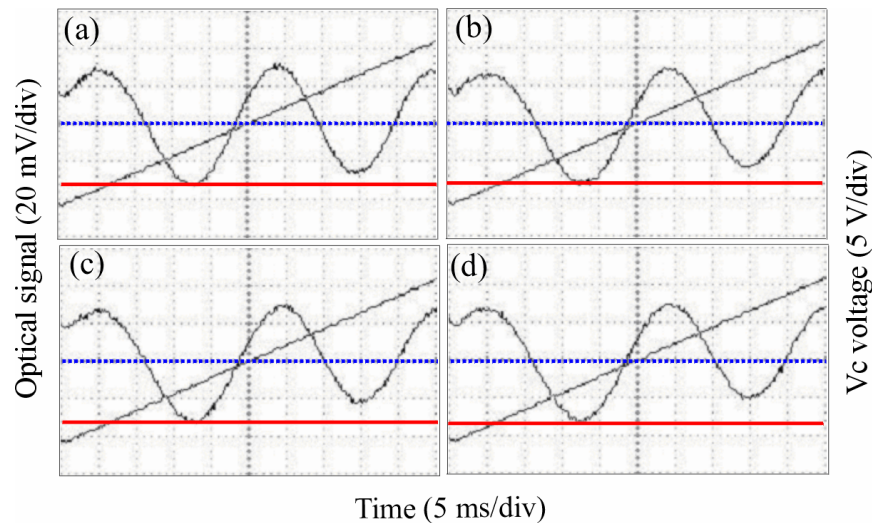


Fig. 4. Long-term stability measurements on the conversion performance at different measured times: (a) 20 min, (b) 40 min, (c) 50 min, and (d) 60 min.

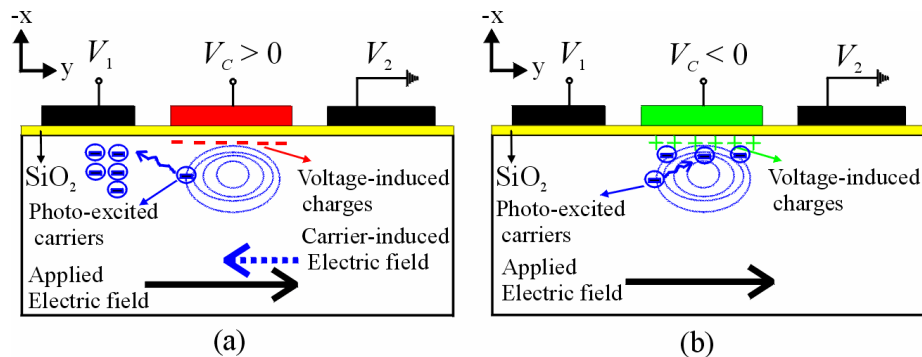


Fig. 5. A schematic explanation for the carrier-induced electric field due to the photorefractive effects: (a)  $V_C > 0$  and (b)  $V_C < 0$ .

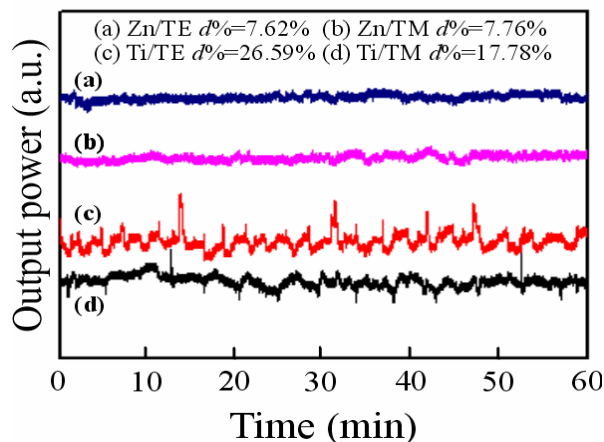


Fig. 6. Optical power variations versus an illuminating time for the Zn-indiffused and the Ti-indiffused channel waveguides at a throughput power of  $80 \mu\text{W}$ .

To compare the optical power-handling stability between the ZI channel waveguide and the conventional TI waveguide on the same LN substrates, a Ti-strip with  $4 \mu\text{m}$ -wide,  $35 \text{ nm}$ -thick, and  $22 \text{ mm}$ -long was thermally diffused at  $1000^\circ\text{C}$  for 4 h in a furnace with the oxygen ambient. The fabricated TI waveguide is single-mode for both TE and TM polarizations. The power variation ( $d\%$ ) is defined as a ratio of power difference between maximum and minimum values to the average values during an observation period of 60 min. A lower power variation indicates that the power stability of channel waveguides is better. Figure 6 illustrates the measurement results for the ZI and the TI channel waveguides under the same throughput power of  $80 \mu\text{W}$  measuring after the output coupling lens. The values of power variation of the ZI waveguides are 7.62% and 7.76% for TE and TM modes, respectively. In contrast, the values of power variation of the TI waveguides are 26.59% and 17.78% for TE and TM modes, respectively. The results show that the ZI waveguides have better power stability than the TI waveguides. Thus, it is expected that the proposed ZI mode converter will have a better performance on the optical power-handling stability than the conventional TI converter, especially in the visible wavelength region.

## 5. Conclusions

We have reported on the first stable Zn-indiffused mode converter in an x-cut/z-propagation lithium niobate. In comparison with the conventional Ti-indiffused converter, a higher optical power throughput and a more stable mode conversion is achievable at a wavelength of  $0.632 \mu\text{m}$ . This technique is very attractive to be used in the integrated waveguide sensors with stable power handling and polarization controlling, especially in the visible wavelength region.

## Acknowledgments

This work was supported in part by the National Science Council, Taiwan, R.O.C., under Grant NSC 95-2221-E-218-076.